

# Two-pion-exchange and other higher-order contributions to the $pp \rightarrow pp\pi^0$ reaction

Y. Kim<sup>(a,b)</sup>, T. Sato<sup>(c)</sup>, F. Myhrer<sup>(a)</sup> and K. Kubodera<sup>(a)</sup>

- (a) Department of Physics and Astronomy, University of South Carolina, Columbia, South Carolina 29208, USA
- (b) School of Physics, Korea Institute for Advanced Study, Seoul 130-012, Korea
- (c) Department of Physics, Osaka University, Toyonaka, Osaka 560-0043, Japan

(March 25, 2022)

## Abstract

Much effort has been invested on effective-field-theoretical studies of the near-threshold  $NN \rightarrow NN\pi$  reactions and, in order to deal with the somewhat large three-momentum transfers involved, the momentum counting scheme (MCS) was proposed as an alternative to the usual Weinberg counting scheme. Given the fact that a quantitative explanation of the existing high-precision  $NN \rightarrow NN\pi$  data requires a careful examination of higher chiral order contributions to the transition operator, we make a detailed numerical investigation of the convergence property of MCS for a pilot case of the  $pp \rightarrow pp\pi^0$  reaction. Our study indicates that MCS is superior to the Weinberg scheme in identifying dominant higher order contributions to the  $NN \rightarrow NN\pi$  reactions.

There exists a substantial accumulation of high-precision data on various observables for the near-threshold  $NN \rightarrow NN\pi$  reactions, e.g. [1], and providing a coherent understanding of these experimental results has been a prominent theoretical challenge, see e.g., [2, 3, 4, 5, 6, 7, 8, 9]. Heavy-baryon chiral perturbation theory (HB $\chi$ PT), which is a low-energy effective field theory of QCD, is expected to offer a systematic framework for describing these reactions. In HB $\chi$ PT, the four-momentum  $Q$  characterizing a given physical process is assumed to be small compared to the chiral scale  $\Lambda_\chi \simeq 4\pi f_\pi \simeq 1$  GeV, and contributions to the transition amplitude are classified according to the power (chiral order) of the expansion parameter  $\epsilon \equiv Q/\Lambda_\chi$ .<sup>1</sup> The coefficients of possible terms in the HB $\chi$ PT Lagrangian, called low-energy constants (LECs), can in principle be linked to the matrix elements of QCD operators but in practice they are determined from experimental observables. Once all the LEC are fixed up to a specified chiral order, HB $\chi$ PT allows us to make predictions for a wide range of hadronic and electroweak processes.

Although, as mentioned, HB $\chi$ PT presupposes the smallness of its expansion parameter  $Q/\Lambda_\chi$ , the pion production reactions involve somewhat large momentum transfers,  $p \simeq \sqrt{m_\pi m_N}$ , even at threshold. This implies that the application of HB $\chi$ PT to the  $NN \rightarrow NN\pi$  reactions may involve some delicate aspects, but this also means that these processes may serve as a good test case for probing the applicability (or the limit of applicability) of HB $\chi$ PT. It is worth emphasizing that finding a valid EFT expansion scheme for the  $NN \rightarrow NN\pi$  reactions is of general importance (going beyond the specific context of the  $NN \rightarrow NN\pi$  reactions) because, once such a scheme is found, we expect to be able to develop similar frameworks for other nuclear processes which involve rather large energy-momentum transfers and hence may not be quite amenable to the straightforward application of the ordinary HB $\chi$ PT approach. To account for the rather large momentum transfers involved in the  $NN \rightarrow NN\pi$  reactions, Cohen, Friar, Miller and van Kolck [5] proposed to replace the ordinary chiral counting scheme of Weinberg (W-scheme) with a new scheme called the momentum counting scheme (MCS). The expansion parameter in MCS is  $\tilde{\epsilon} \equiv p/m_N \simeq (m_\pi/m_N)^{1/2} \simeq 1/2.6$ , which is appreciably larger than the expansion parameter  $\epsilon \simeq m_\pi/m_N \simeq 1/6.7$  in the W-scheme.

Although the formal aspects of MCS have been discussed rather extensively [8], it seems fair to say that its practical utility is yet to be established. An important point to be noted here is that, whereas in the W-scheme a given Feynman diagram

---

<sup>1</sup> The numerical value of the chiral expansion parameter is  $\epsilon \simeq m_\pi/\Lambda_\chi \simeq 1/7.1$ , while the ‘‘recoil-correction’’ expansion parameter is  $m_\pi/m_N \simeq 1/6.7$ . Since these parameters have roughly the same numerical value, the chiral and recoil-correction expansions are combined together in HB $\chi$ PT.

corresponds to a definite power in  $\epsilon$  (it thus has a unique HB $\chi$ PT order), this type of correspondence does not in general exist in MCS, because a given Feynman diagram can involve contributions that belong to different orders in  $\tilde{\epsilon}$ . In the following, the contribution corresponding to the lowest power of  $\tilde{\epsilon}$  for a given diagram is referred to as the “leading term” [7, 8], and the remaining (higher order in  $\tilde{\epsilon}$ ) contributions of the diagram as “sub-leading terms”. It is to be emphasized that, in order to study the convergence property of MCS, we need to examine not only the behavior of the leading terms but also that of the sub-leading terms. Our first attempt at such a study was described in Ref. [10, 11], to be referred to as KSMK1. The results presented in KSMK1 indicate that the individual terms in the MCS expansion exhibit much more complicated behavior than the straightforward power counting in  $\tilde{\epsilon}$  would indicate.

The study in KSMK1, however, is subject to elaboration in at least two points. The first is that, for the nucleon propagator, KSMK1 used the standard HB $\chi$ PT propagator instead of the MCS propagator (see below), and the consequences of this eclectic treatment need to be investigated. The second point is that, in KSMK1, only the nucleons and pions appear as effective degrees of freedom, with the  $\Delta$ -particle field integrated away. In view of the rather high momentum transfers involved in the  $NN \rightarrow NN\pi$  reactions, the influence of including the  $\Delta$ -particle as an explicit degree of freedom is well worth examination. Since however this second point has been discussed in Refs. [8, 12],<sup>2</sup> we concentrate here on the first point. Furthermore, we limit ourselves here to the study of the transition operators (or equivalently the transition amplitudes in plane-wave approximation) even though the actual transition amplitudes need to be calculated with the use of the distorted-waves (DW) for the initial and final two-nucleon systems. Previous studies (see, e.g., [4, 5, 8, 13]) have shown that, in order to reproduce the experimental data, it is crucially important to evaluate higher chiral-order contributions to the transition operator. In the present work, therefore, we focus on the convergence property of the MCS expansion of the transition amplitudes calculated in plane-wave approximation. As mentioned, the  $NN \rightarrow NN\pi$  reactions serve as a pilot case for nuclear reactions that involve rather high energy-momentum transfers, and it is hoped that our present study (despite its stated limitations) will shed some light on the general issue of an effective-field theoretical treatment of those reactions.

Of the various possible isospin channels for the  $NN \rightarrow NN\pi$  reactions, we concentrate (as we did in KSMK1) on the  $pp \rightarrow pp\pi^0$  reaction. The amplitudes for the  $NN \rightarrow NN\pi$  reactions are in general dominated by a pion-rescattering diagram in

---

<sup>2</sup> In Ref. [8] it is convincingly argued that at next-to-leading-order (NLO) in MCS, the diagrams involving a  $\Delta$  cancel for s-wave pion production, i.e.  $\Delta$  will only enter at higher orders in MCS.

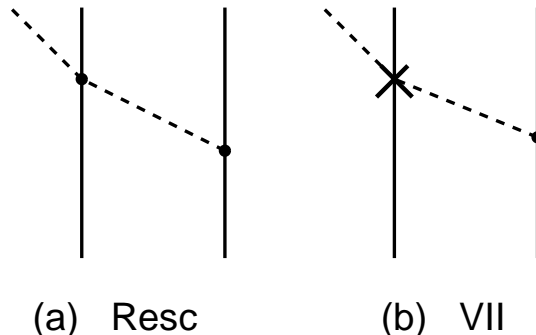


Figure 1: One-pion-exchange rescattering diagrams of order  $\tilde{e}^3$  (in MCS) for the threshold  $pp \rightarrow pp\pi^0$  reaction. Diagram 1(a) represents the lowest-order non-vanishing one-pion-exchange contribution (NLO in the W-scheme), while diagram 1(b) represents its recoil correction (NNLO in the W-scheme). Adopting the same convention as in Ref. [15] for labeling the diagrams, we call diagram 1(a) the *rescattering* diagram, or the *Resc* diagram for short, and refer to diagram 1(b) as diagram VII.<sup>3</sup> The re-scattering vertex in the *Resc* diagram comes from  $\mathcal{L}_{\pi N}^{(2)} = c_1 N^\dagger (\text{Tr}\chi_+) N + \dots$  [16], whereas diagram VII contains the re-scattering (recoil correction) vertex of the next chiral order lagrangian  $\mathcal{L}_{\pi N}^{(3)}$ .

which rescattering is caused by the Weinberg-Tomozawa (WT) interaction term, but this particular diagram does not contribute to the  $pp \rightarrow pp\pi^0$  reaction. This feature makes the  $pp \rightarrow pp\pi^0$  reaction uniquely suited for investigating the behavior of higher order terms in  $s$ -wave pion production.<sup>3</sup>

We have derived in Ref. [15] all the possible two-body transition operators for  $s$ -wave pion production in the  $pp \rightarrow pp\pi^0$  reactions up to next-to-next-to-leading order (NNLO) in the W-scheme.<sup>4</sup> The diagrams generating these operators can be categorized into several groups: the pion-rescattering diagram illustrated in Fig. 1(a) and its recoil correction diagram (diagram VII) shown in Fig. 1(b); the two-pion exchange (TPE) diagrams (diagrams I~IV) in Fig. 2, the vertex loop-correction diagrams (diagrams V and VI) in Fig. 3, and the contact-interaction diagram (CT diagram) in Fig. 4.<sup>5</sup> In what follows, the diagram in Fig.1(a), which specifically represents the

<sup>3</sup> It should be mentioned, however, that the  $s$ -wave pion production amplitude represents a more complicated case than the  $p$ -wave pion production amplitude; the convergence property of MCS for the latter has been discussed in Ref.[14].

<sup>4</sup>The structure of the one-body transition operators is well known in HB $\chi$ PT.

<sup>5</sup>In labeling the diagrams in Figs. 1~4, we are following the same convention as in Ref. [15]; this

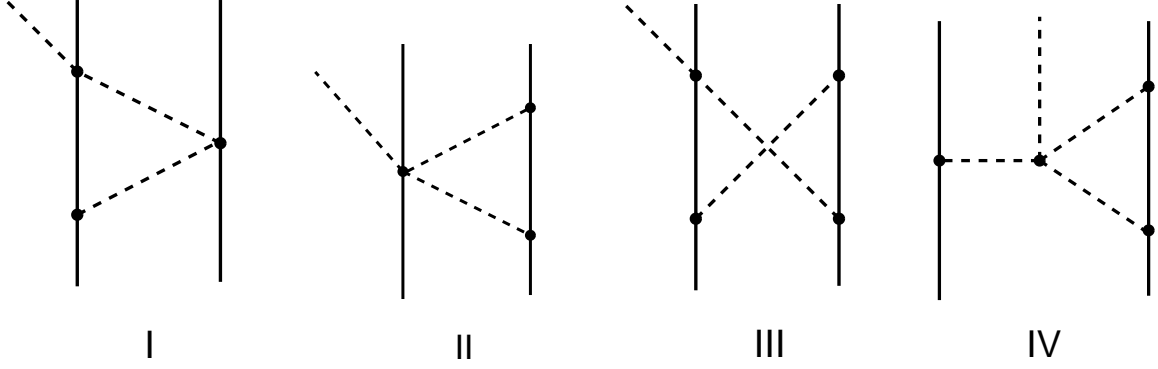


Figure 2: The two-pion-exchange (TPE) diagrams considered to be of order  $\tilde{\epsilon}^2$  in the formal counting in MCS (NNLO in W-scheme). We only show one representative diagram for each group, suppressing similar diagrams belonging to the same group (see Ref. [15] for details). The diagram labels, I, II, III and IV, follow the convention used in Ref. [15]. All the vertices arise from the lowest chiral order lagrangians,  $\mathcal{L}_{\pi N}^{(1)}$  and  $\mathcal{L}_{\pi\pi}^{(2)}$ , see Ref. [16].

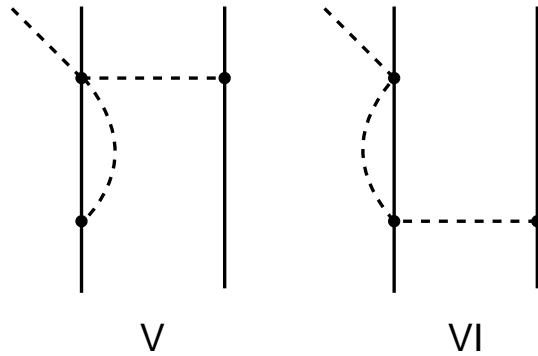


Figure 3: One-pion-exchange diagrams with vertex correction belonging to order  $\tilde{\epsilon}^5$  in MCS (NNLO in the W-scheme). The diagram labels, V and VI, follow the convention used in Ref. [15].

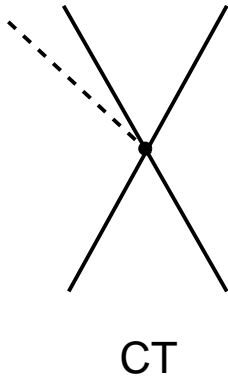


Figure 4: The counter-term (CT) diagram of order  $\tilde{\epsilon}^3$  (NNLO in the W-scheme).

Table 1: The orders of diagrams in the W-scheme and MCS. The labels of the diagrams conform with those used in Ref. [15]. When a diagram is assigned  $\mathcal{O}(\tilde{\epsilon}^n)$  in MCS, it means that its “leading term” is  $\mathcal{O}(\tilde{\epsilon}^n)$  with the understanding that there can also be terms higher order in  $\tilde{\epsilon}$  (“sub-leading terms”).

Diagram	Resc	I	II	III	IV	V	VI	VII	CT
W-scheme	NLO	NNLO	NNLO	NNLO	NNLO	NNLO	NNLO	NNLO	NNLO
MCS	$\mathcal{O}(\tilde{\epsilon}^3)$	$\mathcal{O}(\tilde{\epsilon}^2)$	$\mathcal{O}(\tilde{\epsilon}^2)$	$\mathcal{O}(\tilde{\epsilon}^2)$	$\mathcal{O}(\tilde{\epsilon}^2)$	$\mathcal{O}(\tilde{\epsilon}^5)$	$\mathcal{O}(\tilde{\epsilon}^5)$	$\mathcal{O}(\tilde{\epsilon}^3)$	$\mathcal{O}(\tilde{\epsilon}^3)$

lowest-order non-vanishing one-pion-exchange contribution to  $pp \rightarrow pp\pi^0$ , shall be simply referred to as the *rescattering* diagram, or the *Resc* diagram for short. Table 1 shows the power counting of these diagrams (Figs. 1 ~ 4) in the W-scheme (powers in  $\epsilon$ ) and in MCS (powers in  $\tilde{\epsilon}$ ). The table indicates that the two schemes give significantly different classifications of these diagrams. Diagrams I ~ VII and the CT diagram, which are all categorized as NNLO terms in the W-scheme, belong to different orders in MCS, ranging from  $\mathcal{O}(\tilde{\epsilon}^2)$  to  $\mathcal{O}(\tilde{\epsilon}^5)$ . Furthermore, the Resc term, which in the W-scheme is of NLO and thus of lower chiral order than any other terms in the table, belongs to  $\mathcal{O}(\tilde{\epsilon}^3)$  in MCS, and thus of higher order in  $\tilde{\epsilon}$  than Diagrams I ~ IV. These features invite us to investigate the actual numerical behavior of the

---

leads to a somewhat awkward situation here that the diagrams are not numbered according to the order of their appearance in the text; “diagram VII” shows up earlier than diagrams I, II, III, etc.

diagrams listed in Table 1 in the context of MCS and examine whether MCS indeed provides a useful guide in organizing higher order contributions. The main purpose of this article is to report on such a numerical investigation.

A major difference between the W-scheme [8] and MCS [8] is associated with the different treatments of the nucleon propagator (see e.g. Ref. [16]), and we briefly recapitulate this point here. In HB $\chi$ PT the nucleon momentum  $Q^\mu$  is written as  $Q^\mu = m_N v^\mu + q^\mu$ , where  $m_N$  is the nucleon mass, and  $v^\mu$  is the four-velocity, which may be chosen to be  $v^\mu = (1; \vec{0})$ ; it is assumed that  $|q^\mu| \ll m_N$ . In terms of  $q_\mu$  the Feynman propagator for the heavy nucleon is expressed as

$$S_N(q) = i \frac{Q + m_N}{Q^2 - m_N^2} = i \left( v \cdot q + \frac{q^2}{2m_N} \right)^{-1} \left( \frac{1 + \gamma_0}{2} + \frac{\gamma_0 q_0}{2m_N} - \frac{\vec{\gamma} \cdot \vec{q}}{2m_N} \right). \quad (1)$$

In one version of non-relativistic HB $\chi$ PT, the free heavy-nucleon Lagrangian is chosen in such a manner that the heavy-nucleon propagator is given by

$$S_N(q) = \frac{i}{v \cdot q}, \quad (2)$$

and the difference between the propagators in eqs.(1) and (2) is treated as perturbative recoil corrections which are accounted for in higher chiral order Lagrangians. For convenience, we refer to this approach as the W-scheme.<sup>6</sup> The work in Refs. [11, 15] is based on the use of  $S_N(q)$  given in eq.(2).

Meanwhile, in MCS, one rearranges the expression in eq.(1) to adapt it to a specific kinematic situation pertaining to the  $NN \rightarrow NN\pi$  reaction at threshold. In order for a threshold pion to be produced from two nucleons, the four-momenta of the incoming on-shell nucleons 1 and 2 (in the CM system) with  $m_N v^\mu$  subtracted must be  $p_1 = (m_\pi/2, \vec{p})$  and  $p_2 = (m_\pi/2, -\vec{p})$ , where  $|\vec{p}| = \sqrt{m_N m_\pi + m_\pi^2/4} = \sqrt{m_N m_\pi} [1 + \tilde{\epsilon}^2/8 + \mathcal{O}(\tilde{\epsilon}^4)]$ . (Recall  $\tilde{\epsilon} \equiv \sqrt{m_\pi/m_N}$ .) In what follows, for notational simplicity, we write  $p$  instead of  $p_1$ . When an incoming on-shell nucleon of four-momentum  $p$  produces a pion of four-momentum  $l$ , the off-shell nucleon propagator has a momentum  $p-l$ , where the loop-integral four-momentum  $l$  behaves like:  $v \cdot l = l_0 \sim |\vec{p}| \simeq \sqrt{m_N m_\pi}$ ,  $|\vec{l}| \sim |\vec{p}| \simeq \sqrt{m_N m_\pi}$ . Let the nucleon propagator in eq.(1) be rewritten as

$$S_N(p-l) = i \left( v \cdot (p-l) - \frac{(\vec{p}-\vec{l})^2}{2m_N} + \frac{[v \cdot (p-l)]^2}{2m_N} \right)^{-1} \left( \frac{1 + \gamma_0}{2} - \frac{\vec{\gamma} \cdot (\vec{p}-\vec{l})}{2m_N} + \frac{\gamma_0(p_0 - l_0)}{2m_N} \right)$$

---

<sup>6</sup>It should be remarked, however, that Weinberg [17] discussed problems associated with using the static nucleon propagator, Eq. (2), in the two-nucleon systems, and that he proposed a possible remedy, which however upset the original counting scheme.

$$= i \left( -v \cdot l + v \cdot p - \frac{\vec{p}^2}{2m_N} - \frac{\vec{l}^2 - 2\vec{l} \cdot \vec{p}}{2m_N} + \frac{[p_0 - l_0]^2}{2m_N} \right)^{-1} \left( \frac{1 + \gamma_0}{2} - \frac{\vec{\gamma} \cdot (\vec{p} - \vec{l})}{2m_N} + \frac{\gamma_0(p_0 - l_0)}{2m_N} \right) \quad (3)$$

Since  $v \cdot p = \frac{m_\pi}{2}$  and  $v \cdot l \sim \sqrt{m_N m_\pi}$ , the difference

$$v \cdot p - \frac{\vec{p}^2}{2m_N} = \frac{m_\pi}{2} - \frac{m_N m_\pi (1 + \tilde{\epsilon}^2/4)}{2m_N} = -\sqrt{m_N m_\pi} \frac{\tilde{\epsilon}^3}{8}, \quad (4)$$

appearing in eq.(3) is of higher order in  $\tilde{\epsilon}$  compared to  $v \cdot l$  and the other terms in eq.(3) and therefore can be dropped. This treatment of the  $\vec{p}^2/2m_N$  term is to be contrasted to that in the W-scheme, where the  $\vec{p}^2/2m_N$  term is included in the higher chiral order lagrangian and treated as a perturbative correction. We now reorganize eq.(3) as

$$S_N(p-l) = i \left[ -v \cdot l - \left\{ \frac{\vec{l}^2 - 2\vec{l} \cdot \vec{p}}{2m_N} - \frac{(p_0 - l_0)^2}{2m_N} \right\} \right]^{-1} \left( \frac{1 + \gamma_0}{2} - \frac{\vec{\gamma} \cdot (\vec{p} - \vec{l})}{2m_N} + \frac{\gamma_0(p_0 - l_0)}{2m_N} \right) + \dots \quad (5)$$

Here, compared with the leading term  $v \cdot l$ , the terms in the curly brackets are of order  $\tilde{\epsilon}$  or higher. Expanding eq.(5) in powers of  $1/2m_N$  we arrive at the expression given in appendix B of Ref. [18]:

$$S_N(p-l) = \left( \frac{-i}{v \cdot l} \right) \left[ \frac{1 + \gamma_0}{2} \left\{ 1 - \frac{\vec{l}^2 - 2\vec{l} \cdot \vec{p}}{2m_N l_0} \right\} - \frac{\vec{\gamma} \cdot (\vec{p} - \vec{l})}{2m_N} + \frac{(v \cdot l)}{2m_N} \left( \frac{1 - \gamma_0}{2} \right) \right] + \dots \quad (6)$$

where the three terms containing the factor  $1/2m_N$  are of order  $\tilde{\epsilon}$  relative to 1. In MCS, one applies the lowest-order non-relativistic approximation to eq.(6) (letting  $\gamma_0 \rightarrow 1$  and ignoring the  $\tilde{\epsilon}$  corrections) and adopts as the heavy-nucleon propagator

$$S_N(p-l) = -\frac{i}{v \cdot l} \quad (7)$$

In Ref. [18], the  $1/2m_N$  term within the curly brackets in eq. (6) was classified as a heavy-nucleon propagator recoil correction, while the other two  $1/2m_N$  terms were classified as higher order vertices in the the Lagrangian. In the present work, following Ref. [18], we use eq.(7) without considering these corrections.

We investigate numerical differences in the transition amplitudes resulting from the use of the two different expressions, eqs.(2) and (7), for the nucleon propagator.



As mentioned, the analytic expressions for the  $pp \rightarrow pp\pi^0$  transition operators were calculated in Ref. [15] up to NNLO in the W-scheme [i.e., the HB $\chi$ PT propagator, eq. (2) was used].<sup>7</sup> It turns out that the amplitude expressions in MCS can be readily obtained from those given in Ref. [15]. The dependence on  $v \cdot p$  in the amplitudes enters only through the HB $\chi$ PT propagator eq. (2) with  $q = p - l$ . This implies that the amplitudes resulting from the use of the MCS nucleon propagator, eq. (7), can be simply obtained by formally replacing  $v \cdot p$  with zero ( $v \cdot p \rightarrow 0$ ) in the expressions given in Ref.[15]. These expressions are valid for arbitrary kinematics but, for the present purpose, we simplify them with the use of the *fixed (frozen) kinematics approximation* (FKA), wherein the external energies and momenta appearing in the particle propagators and vertices are “frozen” at their threshold values.

In FKA, the operator corresponding to each of the diagrams in Figs. 1~4 are written as

$$T = \left( \frac{g_A}{f_\pi} \right) (\vec{\Sigma} \cdot \vec{k}) t(p, p', x) \quad (8)$$

where  $\vec{p}$  ( $\vec{p}'$ ) is the relative three-momentum in the initial (final)  $pp$  state ( $\vec{p}_1 - \vec{p}_2 = 2\vec{p}$ ,  $\vec{p}'_1 - \vec{p}'_2 = 2\vec{p}'$ ),  $\vec{k} \equiv \vec{p} - \vec{p}'$ ,  $x = \hat{p} \cdot \hat{p}'$ , and  $\vec{\Sigma} = \frac{1}{2}(\vec{\sigma}_1 - \vec{\sigma}_2)$ . The partial-wave projected form of  $t(p, p', x)$  is written as [13]

$$J[t] = - \left( \frac{m_N m_\pi}{8\pi} \right) \int_0^\infty p^2 dp p'^2 dp' \int_{-1}^1 dx \psi_{1S_0}(p') t(p, p', x) (p - p'x) \psi_{3P_0}(p) \quad (9)$$

where  $\psi_\alpha(p)$  is the  $\alpha$  partial-wave ( $1S_0$  for the initial state and  $3P_0$  for the final state).<sup>8</sup> For the  $t(p, p', x)$ 's corresponding to the two-pion exchange (TPE) diagrams (diagrams I, II, III and IV in Fig. 2), it is informative to decompose each of them into terms with definite *asymptotic*  $k$ -dependence as [11, 19]

$$t(p, p', x) = t_1 (g_A / (8f_\pi^2))^2 |\vec{k}| + t_2 (\ln\{|\vec{k}|^2 / \Lambda^2\}) + t_3 + \delta t(p, p', x), \quad (10)$$

where, in the limit of  $k \rightarrow \infty$ ,  $t_3$  is  $k$ -independent, and  $\delta t(p, p', x)$  is  $\mathcal{O}(k^{-1})$ . The analytic expressions for  $t_i$ 's ( $i = 1, 2, 3$ ) can be extracted [19] from the amplitudes  $T$  given in Ref. [15]. The first term with  $t_1$  in eq.(10) is the “leading part” of  $\mathcal{O}(\tilde{e}^2)$  in MCS, which was evaluated in Ref. [7]; the remaining “sub-leading” terms in eq.(10)

<sup>7</sup> The amplitude for diagram II given in Ref. [15] has the wrong sign.

<sup>8</sup> In this work we adopt the plane-wave approximation, which corresponds to the use of the wave functions of the generic form  $\psi(p) = \delta(p - p_{on})/p^2$ , where  $p_{on}$  is the asymptotic on-shell nucleon momentum.

were not considered in Ref. [7]. For the reason to be explained later, we introduce the “sub-leading” terms of  $\mathcal{O}(\tilde{\epsilon}^3)$  as

$$t^*(p, p', x) \equiv t(p, p', x) - t_1 \left( g_A / (8f_\pi^2) \right)^2 |\vec{k}| \quad (11)$$

and, correspondingly,

$$J[t^*] = - \left( \frac{m_N m_\pi}{8\pi} \right) \int_0^\infty p^2 dp \int_{-1}^1 dx \psi_{1S_0}(p') t^*(p, p', x) (p-p') \psi_{3P_0}(p) \quad (12)$$

We remark that, for diagram I, we have  $t^*(p, p', x) = t(p, p', x)$  and  $J[t^*] = J[t]$ , since the  $t_1$  term exists only for diagrams II, III and IV [11, 19]. In what follows, we investigate the numerical behavior of  $J[t]$  and  $J[t^*]$ . For the sake of definiteness, we concentrate here on a representative near-threshold case where the kinetic energy of the incident proton (in the laboratory system) is  $T_{lab} = 281$  MeV.

We first consider the two-pion exchange (TPE) contributions, coming from diagrams I  $\sim$  IV depicted in Fig. 2. Since the leading parts of the TPE diagrams of  $\mathcal{O}(\tilde{\epsilon}^2)$  are known to cancel among themselves [7, 11],<sup>9</sup> our main concern here is the behavior of  $t^*(p, p', x)$ , eq.(11), or equivalently  $J[t^*]$ , eq.(12). We show in Table 2 the values of  $J[t^*]$  corresponding to each of diagrams I  $\sim$  IV. In the last column we also give  $J[t]_{\text{Resc}}$ , which is the contribution to  $J[t]$  from the rescattering diagram (Resc) (Fig.1). The second row gives  $J[t^*]$  calculated in MCS, while the third row shows  $J[t^*]$  calculated in the W-scheme [11]. Since the rescattering diagram contains no nucleon propagators, the W-scheme and MCS give the same value for  $J[t]_{\text{Resc}}$ . The fourth row gives  $J[t_1]$  representing the contribution of the leading  $t_1$  term; we remark that, for  $J[t_1]$ , both MCS and the W-scheme give the same result. For comparison, we present in the fifth row the value of  $J[t]$  calculated in Ref. [15] with the use of the W-scheme.

Comparison of the  $J[t^*; MCS]$ 's and  $J[t^*; W]$ 's in Table 2 indicates that the different treatments of the heavy-nucleon propagator between the W-scheme and MCS affect rather appreciably the individual values of  $J[t^*]$ 's for diagrams I  $\sim$  IV. Thus, for a formally consistent check of MCS it is important to use the MCS nucleon propagator, and in what follows we shall mostly concentrate on the results obtained with the MCS nucleon propagators.

According to MCS,  $J[t^*]$  for the TPE diagrams should be of  $\mathcal{O}(\tilde{\epsilon}^3)$ , and  $J[t]_{\text{Resc}}$  should also be of  $\mathcal{O}(\tilde{\epsilon}^3)$ , see Table 2. Thus, if MCS is a reasonable counting scheme,

---

<sup>9</sup> This can also be seen in our Table 2. Since  $t_1 = 0 : -1 : -1/2 : 3/2$  for diagram I, II, III and IV, respectively, the  $J[t_1]$ 's in the table are found to be in the ratio of  $0 : -2 : -1 : 3$  and they add up to zero.

Table 2: The  $pp \rightarrow pp\pi^0$  amplitudes  $J$ , eqs. (9) and (12), calculated for  $T_{lab} = 281$  MeV in the plane-wave approximation, and in the frozen kinematics approximation (FKA). The labels, I~IV, correspond to the diagrams I~IV depicted in Fig. 2, while the column labeled “Sum” gives their combined contributions. The last column shows the contribution to  $J[t]$  from the lowest-order non-vanishing one-pion-exchange rescattering diagram, the *Resc* diagram (Fig.1(a)). The second row shows  $J[t^*]$  calculated in MCS and formally of  $\mathcal{O}(\tilde{\epsilon}^3)$ , while the third row gives  $J[t^*]$  evaluated in the W-scheme [15]. The fourth row gives  $J$  coming from the leading  $t_1$  term of MCS order  $\tilde{\epsilon}^2$ ; since  $J[t_1; \text{MCS}] = J[t_1; \text{W}]$  we simply write  $J[t_1]$ . The fifth row gives  $J[t]$  calculated in Ref. [15] with the use of the W-scheme.  $J[t^*; \text{W}] + J[t_1] = J[t; \text{W}]$ , see eq.(11).

Type of diagram	I	II	III	IV	Sum	Resc
$J[t^*; \text{MCS}] \times 10^2$	-1.4	-13.2	-23.1	12.5	-25.2	8
$J[t^*; \text{W}] \times 10^2$	-5.6	-6.5	-29.9	4.9	-37.1	8
$J[t_1] \times 10^2$	0	-46.7	-23.3	70.0	0	
$J[t; \text{W}] \times 10^2$	-5.6	-53.2	-53.2	74.9	-37.1	8

$J[t^*]$  and  $J[t]_{\text{Resc}}$  are expected to be of comparable magnitudes. A comment is in order here, however, on the meaning of “comparable magnitudes”. Usually, two quantities that differ by a factor of 2~3 are considered to be of comparable magnitudes (or of the same order) but, in the present case where the expansion parameter is  $\tilde{\epsilon} \sim 1/3$ , a difference by a factor of  $\sim 3$  may be interpreted as representing a different order in  $\tilde{\epsilon}$ . Ideally speaking, one could make the situation clearer by comparing terms that differ by two orders in  $\tilde{\epsilon}$ . In our present study, however, this is possible only for certain classes of diagrams (these cases will be discussed later in the text). For the other cases in which MCS can be tested only within one order in  $\tilde{\epsilon}$ , we shall adopt the following viewpoint: If a deviation from the behavior expected from MCS lies within a factor of  $\sim 3$ , we categorize it as *reasonably consistent* with MCS, in the sense that the deviation does *not* constitute definitive evidence for a breakdown of MCS.

In looking at Table 2, we first concentrate on diagrams II, III and IV, leaving out diagram I for a while. We note that  $J[t^*; \text{MCS}]$  for diagrams II and IV are close to  $J[t]_{\text{Resc}}$ , while  $J[t^*; \text{MCS}]$  for diagram III is larger than  $J[t]_{\text{Resc}}$  by a factor of  $\sim 3$ .<sup>10</sup> Thus the numerical behavior of the  $J[t^*; \text{MCS}]$ 's for diagrams II, III and IV is either

<sup>10</sup> In what follows, we are mostly concerned with the absolute value of  $J$  rather than  $J$  itself but, for the sake of simplicity, we shall refer to the absolute value of  $J$  simply as  $J$  (when there is no danger of confusion).

Table 3: The  $pp \rightarrow pp\pi^0$  amplitudes  $J[t]$ , eq. (9), calculated for  $T_{lab} = 281$  MeV in the plane-wave approximation and in FKA. The labels, V, VI and VII, correspond to the diagrams V, VI and VII depicted in Figs. 3 and 1, respectively. The last column gives the contribution to  $J[t]$  from of the rescattering diagram (Fig.1). The second and third rows show, respectively,  $J[t]$  calculated in MCS and in the W-scheme [15].

Type of diagram	V	VI	VII	Resc
$J[t; MCS] \times 10^2$	3.4	-2.3	20.8	8
$J[t; W] \times 10^2$	1.4	1.1	20.8	8

consistent or reasonably consistent with MCS. We find a similar situation in comparing  $J[t^*; MCS]$  (second row) and  $J[t_1]$  (fourth row). According to MCS,  $J[t^*]$  should be one order higher in  $\tilde{\epsilon}$  than  $J[t_1]$ . For diagrams II and IV,  $J[t^*; MCS]$ 's exhibit a slight over-suppression (beyond  $\tilde{\epsilon} \sim 1/3$ ) but they are still *reasonably consistent* with MCS. For diagram III,  $J[t^*; MCS] \sim J[t_1]$  and hence no suppression is seen, but the level of deviation from the MCS rule is again within a factor of  $\sim 3$ , presenting another *reasonably consistent* case.

According to Table 2,  $J[t^*; MCS]$  for diagram I is smaller than  $J[t]_{\text{Resc}}$  by a factor of  $\sim 6$ , in contrast to the other TPE diagrams. It is to be noted however that, for diagram I, the leading term itself exhibits an unusual behavior; *viz.*, although a straight-forward MCS counting indicates that diagram I, containing only one nucleon propagator, should be of order  $\tilde{\epsilon}^2$ , the actual calculation shows  $t_1 = 0$  [11].<sup>11</sup> It is thus likely that some (possibly accidental) extra suppression mechanism is at work for diagram I. Since the existence of this type of extra suppression does not necessarily signal a breakdown of a perturbation series, we may take the view that the results for diagram I is essentially consistent with MCS. Based on the above discussion, we conclude that the overall behavior of our numerical results shown in Table 2 is *reasonably consistent* with MCS. As mentioned, we are ignoring here the recoil correction to the MCS propagator eq. (7). We will return to this issue later in the text.

We next discuss the behavior of the other higher-order contributions coming from diagrams V and VI (Fig. 3) and diagram VII (Figs. 1(b)). In diagram VII the pion-nucleon rescattering vertex is given by  $\mathcal{L}_{\pi N}^{(3)}$ , see eq.(C.3) in Ref. [20]; this vertex contains the recoil correction to the pion-nucleon vertex in the lower chiral order re-

---

<sup>11</sup> This corresponds to the remark made in Ref. [7] that diagram I is “beyond next-to-leading order”.

scattering amplitude (*Resc*) in Fig. 1(a). In Table 3 we show  $J[t]$  for diagrams V, VI and VII, calculated in MCS (second row) and in the W-scheme (third row); this latter has been taken from Ref.[15]. According to MCS [8], diagrams V and VI, which are the pion s-wave re-scattering diagrams containing a pion loop at one nucleon vertex, should be suppressed by  $\tilde{\epsilon}^2 \simeq 1/7$  compared to diagram VII. The numerical results in Table 3 are in conformity with this expected suppression. Meanwhile, diagrams VII and *Resc* (shown in Fig.1) should both be of order  $(\tilde{\epsilon})^3$  in MCS [7, 8]. Table 3 indicates that  $J[t]$  for diagram VII is larger than  $J[t]_{\text{Resc}}$  by a factor of  $\sim 3$ , but here again this level of deviation from the MCS prediction is regarded as constituting a *reasonably consistent* case. It is informative to study in more detail the origin of the differences between these two contributions. For threshold kinematics (FKA), the pion-nucleon re-scattering vertices in the *Resc* diagram and diagram VII are given, respectively, by<sup>12</sup>

$$\text{Resc :} \quad -i \frac{m_\pi^2}{f_\pi^2} \left[ 4c_1 - \left( c_2 - \frac{g_A^2}{8m_N} \right) - c_3 \right] \quad (13)$$

$$\text{VII :} \quad i \frac{m_\pi^2}{f_\pi^2} \left[ c_2 \left( 1 + \frac{3m_\pi}{4m_N} \right) - \frac{g_A^2}{16m_N} \right] \quad (14)$$

Formally, these two vertices do seem to be of the same order in MCS. However, the well-known smallness of the  $\pi N$  iso-scalar scattering length requires a substantial cancellation between the three  $c_i$  terms in eq.(13). This particular situation causes the expression in eq.(14) to become larger than that in eq.(13) by almost a factor of 3. These features illustrate intrinsic subtlety we encounter in discussing the convergence property of MCS beyond the level of a factor of  $\sim 3$ . On the other hand, according to the W-scheme, the *Resc* diagram belongs to NLO and diagram VII to NNLO (see Table 1). Our numerical results exhibit a definite deviation from the prediction based on the W-scheme.

We have seen above that, despite the fact that the expansion parameter  $\tilde{\epsilon}$  in MCS is not very small ( $\tilde{\epsilon} \sim 1/3$ ), MCS is likely to provide a useful guide in organizing the higher-order terms. In this connection, it seems worthwhile to examine  $J[t]$  as a function of  $\tilde{\epsilon}$  by allowing  $\tilde{\epsilon}$  to vary from its physical value to smaller values. This may offer information somewhat different from that obtainable by comparing the magnitudes of the individual diagrams at the fixed value of  $\tilde{\epsilon}$ . We explore here how the contributions of the diagrams behave when the pion mass  $m_\pi$  is artificially varied. To extract the non-trivial  $m_\pi$ -dependence of  $J$ , we define the plane-wave amplitude

---

<sup>12</sup> For the vertex for the *Resc* diagram, see eq.(A.29) in Ref. [16]; for the vertex for diagram VII, see eq.(C.3) in Ref. [20].

$X$  by

$$J[t^*] = - \left( \frac{m_N m_\pi}{8\pi} \right) 2|\vec{k}| X \quad (15)$$

As for the “leading term” of the TPE amplitude (viz., the  $t_1$ -term contribution), we take as a representative the  $J[t_1]$  for diagram II and introduce

$$J[t_1; \text{diagram II}] \equiv - \left( \frac{m_N m_\pi}{8\pi} \right) 2|\vec{k}| X_{t_1} \quad (16)$$

which gives ( $t_1 = 1$  for diagram II)

$$X_{t_1} = \left( g_A / (8f_\pi^2) \right)^2 |\vec{k}|. \quad (17)$$

In Table 4 we show as functions of  $m_\pi$  the values of  $X$  for individual diagrams calculated in MCS. The graphical representation of  $X/m_\pi$  as a function of  $m_\pi$  is given in Fig. 5. We expect from eq.(17) that  $X_{t_1} \simeq \sqrt{m_\pi}$  for  $m_\pi \rightarrow 0$ , and the numbers in the second column of Table 4 indicate that this expectation is borne out. According to MCS, the  $X$ 's for diagrams II, VII and the *Resc* diagram are expected to be linear in  $m_\pi$  for  $m_\pi \rightarrow 0$ . The numerical results in Table 4 are in agreement with this MCS expectation. According to Fig. 5, the  $X$ s for the TPE diagrams I, III and IV appear to have a more complex  $m_\pi$  dependence than implied by a naive application of MCS. The  $X$ s here diminish less rapidly for  $m_\pi \rightarrow 0$  than the expected linear dependence on  $m_\pi$ . We remark that in MCS the chiral log factor,  $\ln(m_\pi)$ , which arises from the loops of the TPE diagrams, is treated as a constant factor that does not affect the MCS power counting. Meanwhile, the existence of the  $t_2$ -term in eq.(10) implies that the  $m_\pi$ -dependence in the chiral log can disturb the simple power counting in MCS, and Fig. 5 indicates the chiral log behavior is dominant at low  $m_\pi$  values. Finally, according to MCS, the  $X$ s for diagrams V and VI are expected to vary as  $m_\pi^2$  for  $m_\pi \rightarrow 0$ . Our numerical results indicate that they go to zero faster than  $m_\pi$  but somewhat slower than  $m_\pi^2$ .

Besides the diagrams so far considered, the five-point vertex counter-term diagram (CT diagram) shown in Fig. 4 is also of order  $\tilde{\epsilon}^3$  in MCS [8], and we now give a brief discussion of the numerical behavior of the CT diagram. An aspect that distinguishes this diagram from the others is that the LEC here is an unknown parameter whereas the LECs in the other diagrams are predetermined from separate sources of information. In the absence of experimental data needed to determine the relevant LEC, we rely here on the resonance saturation prescription and use the  $\sigma$ - and  $\omega$ -exchange

Table 4: The plane-wave amplitude  $X$  [eq.(15)] (in units of  $10^{-2}\text{fm}^3$ ) calculated for  $T_{lab} = 281$  MeV in FKA; e.g., the second column gives the values of  $X_{t_1}$ , eq.(17). For the cases where MCS and the W-scheme give different results, MCS is used.

Diagram	$t_1$	$t^*$ : I	$t^*$ : II	$t^*$ : III	$t^*$ : IV	$t$ : Resc	$t$ : V	$t$ : VI	$t$ : VII
$m_\pi = 140$ MeV	92.6	2.7	26.2	45.9	-24.8	-15.7	-6.8	4.6	-41.5
100	77.9	1.5	18.6	43.8	-19.5	-11.6	-3.8	2.6	-29.9
50	54.7	0.3	9.4	32.6	-11.3	-6.1	-1.1	0.8	-15.1
10	24.3	-0.1	2.1	10.9	-2.9	-1.3	-0.06	0.04	-3.1

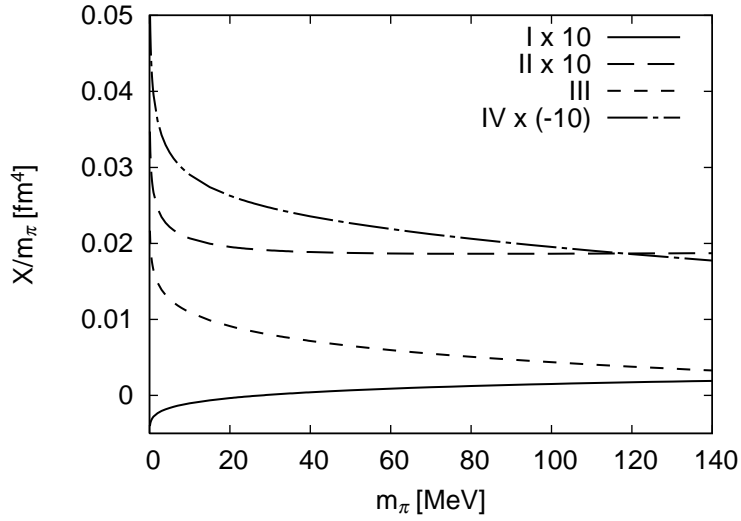


Figure 5: For each of the TPE diagrams,  $X/m_\pi$  is plotted as a function of  $m_\pi$ ; the amplitudes  $X$  are defined in eq.(15).

mechanism considered in Lee and Riska's work [3]. In this model, the amplitude  $T$  [eq.(8)] for the CT diagram is given by, see e.g. Ref. [5]

$$T_{CT} = \frac{g_A \omega_q}{2f_\pi m_N^2} \left[ \left( \frac{g_\sigma^2}{m_\sigma^2} + \frac{g_\omega^2}{m_\omega^2} \right) \vec{\Sigma} \cdot \vec{P} - i \frac{g_\omega^2}{m_\omega^2} (1 + C_\omega) (\vec{\sigma}_1 \times \vec{\sigma}_2) \cdot \vec{k} \right] \quad (18)$$

where  $\omega_q = \sqrt{m_\pi^2 + \vec{q}^2}$  is the energy of the outgoing pion and  $\vec{P} = \vec{p} + \vec{p}'$ .<sup>13</sup> A caveat here is that, since the “ $\sigma$ ” exchange is considered to represent a scalar part of correlated two-pion-exchange in the  $NN$  potential, and since we have already taken into account some TPE diagrams, there is a danger of double-counting if we include the entire “ $\sigma$ ” exchange contribution to the CT diagram. Without going into this issue, we present here the individual contributions of the “ $\sigma$ ”- and  $\omega$ -exchange and compare them with the contributions of the other diagrams that are expected to be of order  $\tilde{\epsilon}^3$  in MCS. If again we restrict ourselves to threshold kinematics ( $\vec{p}' = 0$  and  $\vec{k} = \vec{P} = \vec{p}$ ), eq.(18) can be effectively rewritten as

$$T_{CT} = \left( \frac{g_A}{f_\pi} \right) \vec{\Sigma} \cdot \vec{p} \left( \frac{m_\pi}{2m_N} \right) \left\{ \frac{g_\sigma^2}{m_\sigma^2} + \frac{g_\omega^2}{m_\omega^2} [1 + 2(1 + C_\omega)] \right\} \quad (19)$$

which, with the use of  $g_\sigma^2/(4\pi) = 5$ ,  $g_\omega^2/(4\pi) = 10$ ,  $m_\sigma = 600$  MeV and  $m_\omega = 780$  MeV, leads to

$$T_{CT} = \left( \frac{g_A}{f_\pi} \right) \vec{\Sigma} \cdot \vec{p} \left\{ 13.8 \text{ GeV}^{-3} + 16.4 \text{ GeV}^{-3} [1 + 2(1 + C_\omega)] \right\} \quad (20)$$

Referring to the relation between  $T$  and  $J$ , see eqs. (8) and (9), we estimate  $J_{CT}$  from eq.(20) to be

$$J_{CT} = -0.052 - 0.062 [3 + 2C_\omega] \quad (21)$$

where the first (second) term comes from  $\sigma$ -exchange ( $\omega$ -exchange).<sup>14</sup> The magnitude of the  $J_{CT}$  amplitude is to be compared to  $J(t^*; MCS)$  in the second row in Table 2. Within the factor of  $\sim 3$  the  $\sigma$ - and  $\omega$ -exchange contributions are comparable to the  $\mathcal{O}(\tilde{\epsilon}^3)$  TPE amplitudes in Table 2. Although, as stated earlier, there is a question of

<sup>13</sup> Between the spin singlet and triplet states (between  $^1S_0$  and  $^3P_0$ ), the operator  $i(\vec{\sigma}_1 \times \vec{\sigma}_2)$  is equivalent to  $(-2)\vec{\Sigma}$ .

<sup>14</sup> In the literature we find  $|C_\omega| < 1$  but its value is not well determined; see, e.g., Refs. [21, 22].



possible double-counting concerning the “ $\sigma$ ”-exchange contribution, it is to be noted that the CT amplitude coming from  $\omega$ -exchange alone is of expected MCS magnitude.

To summarize, we have calculated contributions to the threshold  $pp \rightarrow pp\pi^0$  reaction amplitude with the use of the MCS heavy-baryon propagator, studied the convergence property of the expansion based on MCS, and compared the results with those obtained in the W-scheme. We have considered all the diagrams up to NNLO in the W-scheme and, taking advantage of the fact that these diagrams belong to widely different orders in MCS (ranging  $\mathcal{O}(\tilde{\epsilon}^2)$  to  $\mathcal{O}(\tilde{\epsilon}^5)$ ), we have examined whether the actual numerical behavior of these diagrams substantiates the MCS predictions. Our numerical results indicate: (a) The terms that are expected to be of the same order in MCS follow that pattern within a factor of  $\sim 3$ ; (b) The terms that are expected to differ by one order in  $\tilde{\epsilon}$  in MCS also follow that pattern within a factor of  $\sim 3$ ; (c) The terms that are predicted by MCS to be suppressed by two orders in  $\tilde{\epsilon}$  ( $\tilde{\epsilon}^2 \simeq 1/7$ ) clearly show the expected suppression. Thus all the diagrams studied here exhibit numerical behaviors that are (in our definition) *reasonably consistent* [Cases (a) and (b) above], or consistent [Case (c)]. These results lead us to conclude the following (i) Even though the expansion parameter  $\tilde{\epsilon}$  in MCS is not very small ( $\tilde{\epsilon} \sim 1/3$ ), MCS provides a useful semi-quantitative guide in organizing the higher-order terms; (ii) MCS is superior to the W-scheme in organizing the relative importance of the higher order terms. This last conclusion supplements the finding in Ref. [14], which shows that MCS converges for p-wave pion production.

A better test of the convergence property of MCS would be to calculate next-order contributions for all the diagram under consideration and compare the terms that are expected to differ by two orders of  $\tilde{\epsilon}$ , but this is beyond the scope of the present work. As mentioned we have neglected the  $\mathcal{O}(\tilde{\epsilon}^3)$  contributions to the reaction amplitude arising from the recoil correction to the MCS propagator, eq.(7), and we have also ignored the additional vertices discussed in connection eq.(7). We remark, however, that these contributions do not directly affect the behavior of the contributions of the diagrams studied in the present investigation.

Correspondence with C. Hanhart is gratefully acknowledged. This work is supported in part by the US National Science Foundation, Grant Nos. PHY-0457014 and PHY-0758114, and by the Japan Society for the Promotion of Science, Grant-in-Aid for Scientific Research (C) No.20540270.

## References

- [1] H.O. Meyer *et al.*, Phys. Rev. Lett. **65**, 2846 (1990); Nucl. Phys. A, **539**, 633 (1992).
- [2] G.A. Miller and P.U. Sauer, Phys. Rev. C, **44**, R1725 (1991).
- [3] T.-S.H. Lee and D.O. Riska, Phys. Rev. Lett. **70**, 2237 (1993); see also C.J. Horowitz, H. O. Meyer and D.K. Griegel, Phys. Rev. C, **49**, 1337 (1994).
- [4] B.-Y. Park, F. Myhrer, J.R. Morones, T. Meissner and K. Kubodera, Phys. Rev. C, **53**, 1519 (1996).
- [5] T.D. Cohen, J.L. Friar, G.A. Miller and U. van Kolck, Phys. Rev. C, **53**, 2661 (1996).
- [6] S. Ando, T.S. Park and D.P. Min, Phys. Lett. B, **509**, 253 (2001).
- [7] C. Hanhart and N. Kaiser, Phys. Rev. C, **66**, 054005 (2002).
- [8] C. Hanhart, Phys. Rep. **397**, 155 (2004)
- [9] V. Lensky, J. Haidenbauer, C. Hanhart, V. Baru, A. Kudryavtsev and U.-G. Meissner, Eur. Phys. J. A, **27**, 37 (2006) [nucl-th/0511054]; V. Lensky *et al.*, Int.J.Mod.Phys. **A22**, 591 (2007) [nucl-th/0609007].
- [10] F. Myhrer, “Large two-pion-exchange contributions to the  $pp \rightarrow pp\pi^0$  reaction”, in Conf. Proc. *Chiral Dynamics 2006*, eds. M.W. Ahmed, H. Gao, B. Holstein and H.R. Weller (World Scientific, Singapore, 2007), [arXiv:nucl-th/0611051].
- [11] Y. Kim, T. Sato, F. Myhrer and K. Kubodera, Phys. Lett. **B 657**, 187 (2007).
- [12] V. Baru *et al.*, Phys. Lett. B **659**, 184 (2008).
- [13] T. Sato, T.-S.H. Lee, F. Myhrer and K. Kubodera, Phys. Rev. C, **56**, 1246 (1997).
- [14] C. Hanhart, U. van Kolck and G.A. Miller, Phys. Rev. Lett. **85**, 2905 (2000)
- [15] V. Dmitrašinović, K. Kubodera, F. Myhrer and T. Sato, Phys. Lett. B, **465**, 43 (1999).
- [16] V. Bernard, N. Kaiser and U.-G. Meissner, Int. J. Mod. Phys. **E 4**, 193 (1995).

- [17] S. Weinberg, Nucl. Phys. B **363**, 3 (1991)
- [18] C. Hanhart and A. Wirzba, Phys. Lett., **B 650**, 354 (2007)  
[arXiv:nucl-th/0703012].
- [19] T. Sato and F. Myhrer, unpublished notes (1999).
- [20] N. Fettes, U.-G. Meissner and S. Steininger, Nucl. Phys. **A 640**, 199 (1998)  
[arXiv:hep-ph/9803266]
- [21] G. Penner and U. Mosel, Phys. Rev. C **66**, 055211 (2002).
- [22] T. Sato and T.-S. H. Lee, Phys. Rev. C **54**, 2660 (1996).